

Turing pattern selection for a plant-wrack model with cross-diffusion

Ying Sun(孙颖), Jinliang Wang(王进良), You Li(李由), Nan Jiang(江南), and Juandi Xia(夏娟迪)
Citation: Chin. Phys. B, 2023, 32 (**9**): 090203. DOI: 10.1088/1674-1056/acac13
Journal homepage: http://cpb.iphy.ac.cn; http://iopscience.iop.org/cpb

What follows is a list of articles you may be interested in

An incommensurate fractional discrete macroeconomic system: Bifurcation, chaos, and complexity

Abderrahmane Abbes, Adel Ouannas, and Nabil Shawagfeh
Chin. Phys. B, 2023, 32 (**3**): 030203. DOI: 10.1088/1674-1056/ac7296

Bifurcation and dynamics in double-delayed Chua circuits with periodic perturbation

Wenjie Yang(杨文杰)
Chin. Phys. B, 2022, 31 (**2**): 020201. DOI: 10.1088/1674-1056/ac1e0b

Multiple solutions and hysteresis in the flows driven by surface with antisymmetric velocity profile

Xiao-Feng Shi(石晓峰), Dong-Jun Ma(马东军), Zong-Qiang Ma(马宗强), De-Jun Sun(孙德军), and Pei Wang(王裴)
Chin. Phys. B, 2021, 30 (**9**): 090201. DOI: 10.1088/1674-1056/abf7a6

Exact explicit solitary wave and periodic wave solutions and their dynamical behaviors for the Schamel-Korteweg-de Vries equation

Bin He(何斌) and Qing Meng(蒙清)
Chin. Phys. B, 2021, 30 (**6**): 060201. DOI: 10.1088/1674-1056/abd7d1

Bifurcation analysis and exact traveling wave solutions for (2+1)-dimensional generalized modified dispersive water wave equation

Ming Song(宋明)†, Beidan Wang(王贝丹), and Jun Cao(曹军)
Chin. Phys. B, 2020, 29 (**10**): 100206. DOI: 10.1088/1674-1056/ab9f27

Turing pattern selection for a plant–wrack model with cross-diffusion

Ying Sun(孙颖)[1], Jinliang Wang(王进良)[1,†], You Li(李由)[2], Nan Jiang(江南)[1], and Juandi Xia(夏娟迪)[1]

[1] *LMIB and School of Mathematics and Science, Beihang University, Beijing* 100191, *China*
[2] *College of Science, Beijing Forestry University, Beijing* 100083, *China*

(Received 8 October 2022; revised manuscript received 2 December 2022; accepted manuscript online 16 December 2022)

We investigate the Turing instability and pattern formation mechanism of a plant–wrack model with both self-diffusion and cross-diffusion terms. We first study the effect of self-diffusion on the stability of equilibrium. We then derive the conditions for the occurrence of the Turing patterns induced by cross-diffusion based on self-diffusion stability. Next, we analyze the pattern selection by using the amplitude equation and obtain the exact parameter ranges of different types of patterns, including stripe patterns, hexagonal patterns and mixed states. Finally, numerical simulations confirm the theoretical results.

Keywords: plant–wrack model, cross-diffusion, Turing instability, pattern selection, amplitude equation

PACS: 02.30.Oz, 02.30.Hq **DOI:** 10.1088/1674-1056/acac13

1. Introduction

As one of the important branches of nonlinear science, pattern dynamics aims to explore the basic dynamic laws that exist among various ecological systems.[1,2] Patterns are nonuniform macroscopic structures with a certain regularity in space or time and are ubiquitous in nature.[3] Therefore, understanding the causes and mechanism of pattern production is of great importance for uncovering the mystery of natural formation.[4–7]

Plant and wrack are of great significance for protecting the ecology of freshwater wetland. For example, the spatial distribution of plant and wrack can provide a habitat for small animals.[8] In this ecosystem, we observe that little haystacks grow on top of the old ones; these may be induced by diffusion and the interaction of promotion and inhibition of plant and wrack. Therefore, Koppel proposed a reaction–diffusion model

$$\begin{cases} \dfrac{\partial P(t,x,y)}{\partial t} = P(1-P) - sP - iPW\dfrac{k_3}{P+k_3} + d_P\nabla^2 P, \\ t>0,\ \ (x,y)\in\Omega, \\ \dfrac{\partial W(t,x,y)}{\partial t} = sP - bW + d_W\nabla^2 W,\ \ t>0,\ \ (x,y)\in\Omega, \\ \dfrac{\partial P}{\partial \boldsymbol{n}} = \dfrac{\partial W}{\partial \boldsymbol{n}} = 0,\ \ t>0,\ \ (x,y)\in\Omega, \\ P(0,x,y)\geq 0,\ \ W(0,x,y)\geq 0,\ \ (x,y)\in\Omega=[0,L]\times[0,L], \end{cases} \tag{1}$$

to study and explain the regular spatial patterns.[9]

The biological meanings of the variables and parameters of system (1) are as follows: $P(t,x,y)$ and $W(t,x,y)$ are plant biomass and wrack biomass at time t and spatial position (x,y), respectively; $iPW\frac{k_3}{P+k_3}$ describes the inhibition effect of wrack on plant growth; k_3 stands for the level of plant biomass at which inhibition is reduced by half; i is a constant that converts wrack biomass into specific plant growth inhibition; the positive number b indicates the decay rate of wrack; s represents the plant decay rate; d_P and d_W are the positive self-diffusion coefficients of plant and wrack, respectively. Ω is a bounded domain in $\mathbb{R}^2$ with the smooth boundary $\partial\Omega$ and ∇^2 represents the Laplacian operator in two-dimensional space. $\boldsymbol{n}$ is the outward unit normal vector on $\partial\Omega$ and $1/\partial\boldsymbol{n}$ denotes the operator of the directional derivative along the direction $\boldsymbol{n}$.

Many researchers have investigated system (1). Yu derived the mathematical expressions of Hopf bifurcation and the Turing bifurcation boundary and located the Turing bifurcation domain in parameter space; it was found that the typical plant dynamics involves the formation of isolated groups, namely spots, labyrinths and a mixture of stripes and spots, which explained the appearance of the Turing pattern.[10] Liu *et al.* also gave the Turing region in parameter space, and discovered the self-organization behavior between plant and wrack, which induced the formation of a spot pattern.[11] Wang *et al.* carried out theoretical analysis and numerical simulation on model (1) and found that the layer structure of the pattern was induced by the simultaneous instability of the periodic solution with a large amplitude and equilibrium point.[12] Hou *et al.* studied pattern formation mechanisms arising from the interactions between plant and wrack, and gave the conditions for the existence of the patterns.[13] Li *et al.* investigated the spatiotemporal patterns of a freshwater tussock sedge model (1) with discrete time and space variables. They obtained that stable homogeneous solutions can experience Turing instability under certain conditions.[14] For more works about model (1), one can refer to Ref. [15] and the references therein.

Most of the work on biological models has focused on self-diffusion; however, cross-diffusion also plays an impor-

†Corresponding author. E-mail: jlwang@buaa.edu.cn

© 2023 Chinese Physical Society and IOP Publishing Ltd

tant role in many biomasses and is more practical. Kerner mentioned the practical implications of cross-diffusion, and subsequently cross-diffusion in biological models attracted the attention of many scholars.[16] So far, cross-diffusion has been applied to population dynamics, competitive population models and prey–predator models, etc.[17–26] Iida and Banerjee and their colleagues considered the effect of movement of individual prey on predator populations, and introduced a cross-diffusion term of the $\nabla^2(uv)$ type into their model.[27,28] For more about the effects of cross-diffusion, one can refer to Refs. [29–37]. In the biological sense, there exists cross-diffusion between plant and wrack, as the two can promote or inhibit each other. Moreover, few results have been reported regarding cross-diffusion and pattern selection in the plant–wrack model, so we introduce a cross-diffusion term $\nabla^2 P$ into the second equation of model (1), and the cross-diffusion coefficient is denoted by d:

$$\begin{cases} \dfrac{\partial P(t,x,y)}{\partial t} = P(1-P) - sP - iPW\dfrac{k_3}{P+k_3} + d_P\nabla^2 P, \\ t>0,\ \ (x,y)\in\Omega, \\ \dfrac{\partial W(t,x,y)}{\partial t} = sP - bW + d\nabla^2 P + d_W\nabla^2 W, \\ t>0,\ \ (x,y)\in\Omega, \\ \dfrac{\partial P}{\partial \boldsymbol{n}} = \dfrac{\partial W}{\partial \boldsymbol{n}} = 0,\ \ t>0,\ \ (x,y)\in\Omega, \\ P(0,x,y)\geq 0,\ \ W(0,x,y)\geq 0,\ \ (x,y)\in\Omega=[0,L]\times[0,L]. \end{cases} \tag{2}$$

Set $u=\frac{P}{k_3}$, $v=\frac{bW}{k_3 s}$, $\bar{t}=bt$, $a=\frac{1-s}{b}$, $K=\frac{1-s}{k_3}$, $\overline{k_3}=\frac{k_3 is}{b^2}$, $D_1=\frac{d_P}{b}$, $D_2=\frac{d_W}{b}$, $\overline{d}=\frac{d}{s}$ and drop the bar over t, k_3 and d. For convenience, let $a=Ak_3$, then we get the following system:

$$\begin{cases} \dfrac{\partial u(t,x,y)}{\partial t} = k_3\left[Au\left(1-\dfrac{u}{K}\right) - \dfrac{uv}{u+1}\right] + D_1\nabla^2 u, \\ t>0,\ \ (x,y)\in\Omega, \\ \dfrac{\partial v(t,x,y)}{\partial t} = u - v + d\nabla^2 u + D_2\nabla^2 v,\ \ t>0,\ \ (x,y)\in\Omega, \\ \dfrac{\partial u}{\partial \boldsymbol{n}} = \dfrac{\partial v}{\partial \boldsymbol{n}} = 0,\ \ t>0,\ \ (x,y)\in\Omega, \\ u(0,x,y)\geq 0,\ \ v(0,x,y)\geq 0,\ \ (x,y)\in\Omega=[0,L]\times[0,L]. \end{cases} \tag{3}$$

In this paper, our main aim is to study the pattern selection of system (3) through multiple-scale analysis theory, which can give not only the general form of the amplitude equation near the bifurcation point but also determine the corresponding relationship between coefficient and control parameter of the system. Thus, we can know which control parameters of the system are effective. Then we can estimate the effective region of the amplitude equation and study the specific process of the pattern formation in a system with change in the control parameters.

The paper is organized as follows. In Section 2, we investigate the system and conclude that cross-diffusion leads to Turing instability. In Section 3, we obtain the amplitude equation of the Turing pattern at the Turing bifurcation point and obtain the theorem of pattern selection. In Section 4, we verify the correctness of our theoretical analysis through numerical simulations. Finally, in Section 5, a brief conclusion is presented.

2. Turing instability of the system

In this section, we focus on the Turing instability of the system (3). Before starting our research, we first require that the positive equilibrium of the ordinary differential equation (ODE) system is stable.

We consider the ODE system associated with system (3), namely, the non-spatial system in the absence of diffusion terms

$$\begin{cases} \dfrac{\mathrm{d}u}{\mathrm{d}t} = k_3\left[Au\left(1-\dfrac{u}{K}\right) - \dfrac{uv}{u+1}\right], \\ \dfrac{\mathrm{d}v}{\mathrm{d}t} = u - v. \end{cases} \tag{4}$$

In the following, we perform stability analysis for system (4) and obtain the stability theorem.

Theorem 1 [Wang *et al.*, 2019] There are two nonnegative equilibria $E_0=(0,0)$ and $E_*=(u_*,u_*)$ in system (4).

(i) The equilibrium E_0 is a saddle.

(ii) The positive equilibrium E_* is a sink, when one of the following conditions is satisfied: (a) $0<K\leq 1$. (b) $K>1, A\geq A_0$. (c) $K>1, 0<A<A_0, 0<k_3<k_h$.

(iii) The positive equilibrium E_* is a source, when the following condition is satisfied: (d) $K>1, 0<A<A_0, k_3>k_h$.

Here $u_*=\frac{-(A+K-AK)+p}{2A}>0$, $p=\sqrt{(A+K-AK)^2+4A^2K}$, $A_0=\frac{2K(K-1)}{(K+1)^2}$ and $k_h=\frac{K(1+u_*)}{(K-p)u_*}$.

In the following, we study Turing instability of the system with diffusion terms.

2.1. Turing instability for a system with self-diffusion

In this part, we will discuss the Turing instability for the system (3) with self-diffusion (i.e., $d=0$), that is

$$\begin{cases} \dfrac{\partial u}{\partial t} = k_3\left[Au\left(1-\dfrac{u}{K}\right) - \dfrac{uv}{u+1}\right] + D_1\nabla^2 u, \\ \dfrac{\partial v}{\partial t} = u - v + D_2\nabla^2 v. \end{cases} \tag{5}$$

Linearizing system (5) at the positive equilibrium E_*, we have

$$\dot{\boldsymbol{w}} = \boldsymbol{J}_{E_*}\boldsymbol{w} + \begin{pmatrix} D_1 & 0 \\ 0 & D_2 \end{pmatrix}\nabla^2\boldsymbol{w}, \tag{6}$$

where

$$\boldsymbol{w} = \begin{pmatrix} u-u_* \\ v-u_* \end{pmatrix},\ \ \boldsymbol{J}_{E_*} = \begin{pmatrix} a_{11} & a_{12} \\ a_{21} & a_{22} \end{pmatrix},\ \ a_{11} = \frac{k_3 u_*(K-p)}{K(1+u_*)},$$
$$a_{12} = -\frac{k_3 u_*}{1+u_*},\ \ a_{21}=1,\ \ a_{22}=-1. \tag{7}$$

Obviously, the trace and the determinant have the following forms:

$$\mathrm{Tr}(\boldsymbol{J}_{E_*}) = \frac{k_3 u_*(K-p)}{K(1+u_*)} - 1, \ \ \mathrm{Det}(\boldsymbol{J}_{E_*}) = \frac{k_3 u_* p}{K(1+u_*)}.$$

Next, we consider the solution of the system (6) with the following form:

$$\boldsymbol{w} = \begin{pmatrix} c_k^1 \\ c_k^2 \end{pmatrix} \mathrm{e}^{\lambda t + \mathrm{i}\boldsymbol{k}\cdot\boldsymbol{r}}, \tag{8}$$

where $\boldsymbol{k} = (k_x, k_y)$, $\boldsymbol{k}\cdot\boldsymbol{k} = k^2$, $\boldsymbol{r} = (x, y)$ represents the spatial vector in two-dimensional space, k_x and k_y are the wave numbers of the solution, λ represents the growth of disturbance in time t and i represents the imaginary unit, that is, $\mathrm{i}^2 = -1$. Now, substituting Eq. (8) into Eq. (6), we have

$$\lambda^2 - \mathrm{Tr}[\boldsymbol{J}(k)]\lambda + \mathrm{Det}[\boldsymbol{J}(k)] = 0, \tag{9}$$

where

$$\boldsymbol{J}(k) = \boldsymbol{J}_{E_*} - k^2 \begin{pmatrix} D_1 & 0 \\ 0 & D_2 \end{pmatrix},$$

$$\mathrm{Tr}[\boldsymbol{J}(k)] = \mathrm{Tr}(\boldsymbol{J}_{E_*}) - k^2(D_1 + D_2),$$

$$\mathrm{Det}[\boldsymbol{J}(k)] = D_1 D_2 k^4 - k^2(a_{11}D_2 + a_{22}D_1) + \mathrm{Det}(\boldsymbol{J}_{E_*}).$$

In the following, we give stability results for the system (5).

Theorem 2

(I) The positive equilibrium E_* of the system (5) is locally asymptotically stable when one of the following conditions is satisfied: (a) $0 < K \le 1$. (b) $K > 1, A \ge A_0$. (c) $K > 1, 0 < A < A_0, 0 < k_3 < k_h, D_2/D_1 < m_2$.

(II) The positive equilibrium E_* of the system (5) is unstable provided the following condition is satisfied: (d) $K > 1, 0 < A < A_0, 0 < k_3 < k_h, D_2/D_1 > m_2$. Turing bifurcation occurs at $D_2/D_1 = m_2$, where $A_0 = \frac{2K(K-1)}{(K+1)^2}$, $k_h = \frac{K(1+u_*)}{(K-p)u_*}$ and m_2 can be found in the proof of the theorem.

Proof Suppose condition (ii) of Theorem 1 holds. When condition (ii-a) or (ii-b) is satisfied, then $a_{11} \le 0$. So $\mathrm{Det}[\boldsymbol{J}(k)] > \mathrm{Det}(\boldsymbol{J}_{E_*}) > 0$ and the equilibrium E_* is still stable. When condition (ii-c) of Theorem 1 is satisfied, then $0 < a_{11} < 1$. We want to determine the sign of $\mathrm{Det}[\boldsymbol{J}(k)]$, which can be viewed as a quadratic trinomial of k^2. The discriminant

$$\begin{aligned} \Delta &= (a_{11}D_2 + a_{22}D_1)^2 - 4D_1D_2\mathrm{Det}(\boldsymbol{J}_{E_*}) \\ &= D_1^2\left(a_{11}^2\frac{D_2^2}{D_1^2} - 2(a_{11}a_{22} - 2a_{12}a_{21})\frac{D_2}{D_1} + a_{22}^2\right), \end{aligned}$$

where a_{11}, a_{12}, a_{21}, a_{22} are given by Eq. (7). Clearly $-a_{11}a_{22} + 2a_{12}a_{21} < 0$, and $(a_{11}a_{22} - 2\mathrm{Det}(\boldsymbol{J}_{E_*}))^2 - (a_{11}a_{22})^2 > 0$. Thus, Δ can be viewed as a quadratic trinomial of D_2/D_1, and it has two positive roots

$$m_2 = m_0 + 2\sqrt{\mathrm{Det}(\boldsymbol{J}_{E_*})}\frac{\sqrt{\mathrm{Det}(\boldsymbol{J}_{E_*})} + \sqrt{-a_{12}a_{21}}}{a_{11}^2} > m_0,$$

$$m_1 = m_0 - \frac{2m_0\sqrt{\mathrm{Det}(\boldsymbol{J}_{E_*})}}{\sqrt{\mathrm{Det}(\boldsymbol{J}_{E_*})} + \sqrt{-a_{12}a_{21}}} < m_0,$$

where $m_0 = -a_{22}/a_{11} > 0$.

Assume that $a_{11}D_2 + a_{22}D_1 \le 0$, namely, $D_2/D_1 \le m_0$. Then we have $\mathrm{Det}[\boldsymbol{J}(k)] > \mathrm{Det}(\boldsymbol{J}_{E_*}) > 0$, so the equilibrium E_* is still stable.

Assume that $a_{11}D_2 + a_{22}D_1 > 0$, namely, $D_2/D_1 > m_0$. When $m_0 < D_2/D_1 < m_2$, then we have $\mathrm{Det}[\boldsymbol{J}(k)] > 0$, so the positive equilibrium E_* of the system (5) is still stable. When $D_2/D_1 = m_2$ and $k^2 \ne k_c^2 = \frac{a_{11}D_2 + a_{22}D_1}{2D_1D_2}$, we have $\mathrm{Det}[\boldsymbol{J}(k)] > 0$, so the positive equilibrium E_* of the system (5) is still stable. When $D_2/D_1 > m_2$, $\exists k^2$, s.t. $\mathrm{Det}[\boldsymbol{J}(k)] < 0$, so the positive equilibrium E_* of the system (5) is unstable and Turing instability occurs.

2.2. Turing instability for systems with self-diffusion and cross-diffusion

In this section, when a system with a self-diffusion term is stable, we study the Turing instability induced by cross-diffusion in the system (3). Linearizing system (3) at the positive equilibrium E_*, we have

$$\dot{\boldsymbol{w}} = \boldsymbol{J}_{E_*}\boldsymbol{w} + \begin{pmatrix} D_1 & 0 \\ d & D_2 \end{pmatrix}\nabla^2\boldsymbol{w}, \tag{10}$$

where $\boldsymbol{w} = \begin{pmatrix} u - u_* \\ v - u_* \end{pmatrix}$, $\boldsymbol{J}_{E_*} = \begin{pmatrix} a_{11} & a_{12} \\ a_{21} & a_{22} \end{pmatrix}$, and a_{11}, a_{12}, a_{21}, a_{22} are given by Eq. (7).

Considering the form of the solution

$$\boldsymbol{w} = \begin{pmatrix} c_k^1 \\ c_k^2 \end{pmatrix} \mathrm{e}^{\lambda t + \mathrm{i}\boldsymbol{k}\cdot\boldsymbol{r}}. \tag{11}$$

Next, substituting Eq. (11) into Eq. (10), we obtain the dispersion relation

$$\lambda^2 - \mathrm{Tr}[\boldsymbol{J}_1(k)]\lambda + \mathrm{Det}[\boldsymbol{J}_1(k)] = 0, \tag{12}$$

where

$$\boldsymbol{J}_1(k) = \boldsymbol{J}_{E_*} - k^2 \begin{pmatrix} D_1 & 0 \\ d & D_2 \end{pmatrix},$$

$$\mathrm{Tr}[\boldsymbol{J}_1(k)] = \mathrm{Tr}(\boldsymbol{J}_{E_*}) - k^2(D_1 + D_2),$$

$$\mathrm{Det}[\boldsymbol{J}_1(k)] = \mathrm{Det}[\boldsymbol{J}(k)] + da_{12}k^2 = D_1D_2k^4 + qk^2 + \mathrm{Det}(\boldsymbol{J}_{E_*}),$$

$$q = da_{12} - a_{11}D_2 - a_{22}D_1.$$

Based on the condition of self-diffusion stability, together with the analysis of its stability when cross-diffusion is added, we can obtain the following results:

Theorem 3 Suppose condition (I) of Theorem 2 holds. Then we have

(1) The positive equilibrium E_* of the system (3) is locally asymptotically stable, when one of the following conditions is satisfied: (H1) $d = d_c$, $\forall k^2 \ne k_c^2$. (H2) $d > d_c$, $0 < k^2 < \bar{k}_1^2$ or $k^2 > \bar{k}_2^2$. (H3) $d < d_c$.

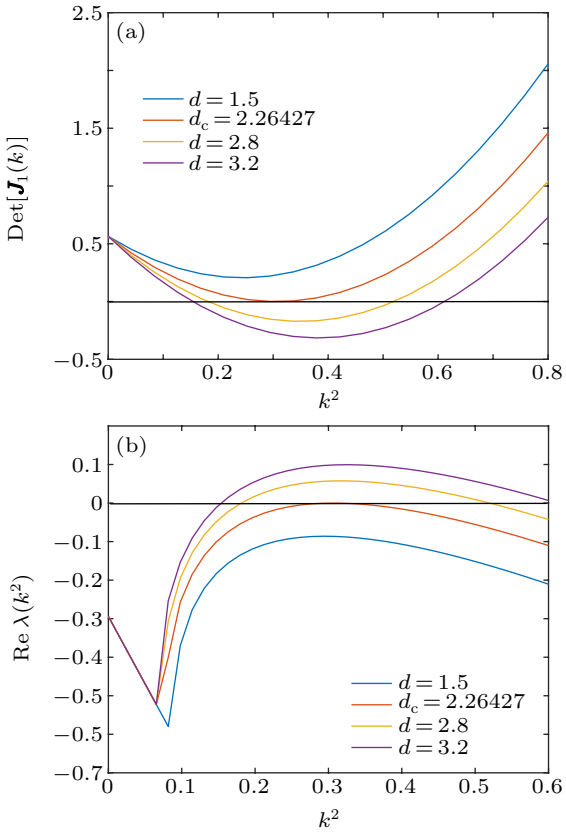


Fig. 1. (a) Function images of $\mathrm{Det}[\boldsymbol{J}_1(k)]$ with k^2 under different cross-diffusion coefficients d. (b) The real part of the largest value as a function of k^2, where $d_c = 2.26427$ (orange), $d = 1.5$ (blue), $d = 2.8$ (yellow) and $d = 3.2$ (purple). The other parameter values are selected as $k_3 = 1.5$, $A = 0.8$, $K = 10$, $D_1 = 1$ and $D_2 = 6$.

(2) The positive equilibrium E_* of the system (3) is unstable provided the following condition holds: (H4) $d > d_c$, $\bar{k}_1^2 < k^2 < \bar{k}_2^2$. Turing bifurcation occurs at $k^2 = \bar{k}_1^2$ or $\bar{k}_2^2$, where k_c^2, d_c, k_1^2 and k_2^2 can be found in the proof of the theorem.

Proof The stability of E_* depends on the sign of $\mathrm{Det}[\boldsymbol{J}_1(k)]$, so we want to determine the sign of $\mathrm{Det}[\boldsymbol{J}_1(k)]$, which can be viewed as a quadratic trinomial of k^2.

Assume that $a_{11}D_2 + a_{22}D_1 - da_{12} \le 0$, namely $d \le \frac{a_{11}D_2+a_{22}D_1}{a_{12}}$. Then we have $\mathrm{Det}[\boldsymbol{J}_1(k)] > 0$, so the equilibrium E_* is still stable.

Assume that $a_{11}D_2 + a_{22}D_1 - da_{12} > 0$, namely $d > \frac{a_{11}D_2+a_{22}D_1}{a_{12}}$. Then we discuss the sign of $\mathrm{Det}[\boldsymbol{J}_1(k)]$: $\mathrm{Det}[\boldsymbol{J}_1(k)]$ reaches its minimum value at $k^2 = k_c^2$, where $k_c^2 = -\frac{q}{2D_1D_2} > 0$. Then we consider the critical condition of $\mathrm{Det}[\boldsymbol{J}_1(k)]$,

$$\min \mathrm{Det}[\boldsymbol{J}_1(k)] = \mathrm{Det}[\boldsymbol{J}_1(k_c)] = 0, \tag{13}$$

and set $q = -\gamma d + \delta$, where $\gamma = -a_{12}$, $\delta = -a_{11}D_2 - a_{22}D_1$. Then substituting it into the second equality of Eq. (13):

$$\frac{-q^2}{4D_1D_2} + \det(\boldsymbol{J}_{E_*}) = 0. \tag{14}$$

Clearly, equation (14) has a negative root, denoted by q_*, then we define $d_c = \frac{\delta - q_*}{\gamma}$.

When $d = d_c$, namely $q = q_*$, we obtain $\mathrm{Det}[\boldsymbol{J}_1(k_c)] = 0$, then $\mathrm{Det}[\boldsymbol{J}_1(k)] > 0$, $\forall k^2 \neq k_c^2$, and the positive equilibrium E_* of the system (3) is still stable.

When $d > d_c$, namely $q < q_* < 0$, we get $\mathrm{Det}[\boldsymbol{J}_1(k_c)] < 0$, then it has two positive roots

$$\bar{k}_{1,2}^2 = \frac{-q \pm \sqrt{q^2 - 4D_1D_2\det(\boldsymbol{J}_{E_*})}}{2D_1D_2}.$$

When $0 < k^2 < \bar{k}_1^2$ or $k^2 > \bar{k}_2^2$ we have $\mathrm{Det}[\boldsymbol{J}_1(k)] > 0$, and the positive equilibrium E_* of the system (3) is still stable. When $\bar{k}_1^2 < k^2 < \bar{k}_2^2$ we have $\mathrm{Det}[\boldsymbol{J}_1(k)] < 0$, and the positive equilibrium E_* of the system (3) is unstable.

When $d < d_c$, namely $q_* < q < 0$, we have $\mathrm{Det}[\boldsymbol{J}_1(k)] > 0$, and the positive equilibrium E_* of the system (3) is still stable.

In the next section, we discuss the amplitude equations of Turing patterns at $d = d_c$.

3. The amplitude equations of the Turing pattern

In this section, we think about the amplitude equations of Turing pattern at $d = d_c$. Considering system (3) that includes self-diffusion and cross-diffusion terms, we use three steps to get the amplitude equations.

Step 1 We consider the perturbation solution $(u - u_*, v - u_*)^{\mathrm{T}}$ of system (3), and we have

$$\begin{cases} \dfrac{\partial u}{\partial t} = D_1\nabla^2 u + a_{11}u + a_{12}v + \dfrac{1}{2}b_{20}u^2 + b_{11}uv \\ \qquad\qquad + \dfrac{1}{2}b_{21}u^2v + \dfrac{1}{6}b_{30}u^3 + o(4), \\ \dfrac{\partial v}{\partial t} = d\nabla^2 u + D_2\nabla^2 v + a_{21}u + a_{22}v, \end{cases} \tag{15}$$

where

$$a_{11} = \frac{k_3u_*(K-p)}{K(1+u_*)},\quad a_{12} = k_3\left(-\frac{u_*}{1+u_*}\right),$$
$$b_{20} = k_3\left(-\frac{2A}{K} + \frac{2u_*}{(1+u_*)^3}\right),\quad b_{11} = k_3\left(-\frac{1}{(1+u_*)^2}\right),$$
$$b_{30} = k_3\left(-\frac{6u_*}{(1+u_*)^4}\right),\quad b_{21} = k_3\left(\frac{2}{(1+u_*)^3}\right),$$
$$a_{21} = 1,\quad a_{22} = -1.$$

Let $\boldsymbol{U} = (u, v)^{\mathrm{T}}$, and system (15) can be transformed into the following system:

$$\frac{\partial \boldsymbol{U}}{\partial t} = \boldsymbol{L}\boldsymbol{U} + \boldsymbol{N}, \tag{16}$$

where

$$\boldsymbol{L} = \begin{pmatrix} D_1\nabla^2 + a_{11} & a_{12} \\ a_{21} + d\nabla^2 & D_2\nabla^2 + a_{22} \end{pmatrix},$$
$$\boldsymbol{N} = \begin{pmatrix} \dfrac{1}{2}b_{20}u^2 + b_{11}uv + \dfrac{1}{2}b_{21}u^2v + \dfrac{1}{6}b_{30}u^3 + o(4) \\ 0 \end{pmatrix}.$$

Let

$$\boldsymbol{L} = \boldsymbol{L}_c + (d - d_c)\boldsymbol{M} = \begin{pmatrix} D_1\nabla^2 + a_{11} & a_{12} \\ a_{21} + d_c\nabla^2 & D_2\nabla^2 + a_{22} \end{pmatrix}$$

$$+(d-d_{\rm c})\begin{pmatrix}0 & 0\\ \nabla^2 & 0\end{pmatrix}. \tag{17}$$

Step 2 We expand the solution of system (3) with a small parameter ε as follows:

$$\boldsymbol{U}=\varepsilon\begin{pmatrix}u_1\\ v_1\end{pmatrix}+\varepsilon^2\begin{pmatrix}u_2\\ v_2\end{pmatrix}+\varepsilon^3\begin{pmatrix}u_3\\ v_3\end{pmatrix}+o(4), \tag{18}$$

$$d-d_{\rm c}=\varepsilon d_1+\varepsilon^2 d_2+\varepsilon^3 d_3+o(4), \tag{19}$$

$$\boldsymbol{N}=\varepsilon^2\boldsymbol{h}_2+\varepsilon^3\boldsymbol{h}_3+o(4), \tag{20}$$

where

$$\boldsymbol{h_2}=\begin{pmatrix}\frac{1}{2}b_{20}u_1^2+b_{11}u_1v_1\\ 0\end{pmatrix},$$

$$\boldsymbol{h_3}=\begin{pmatrix}b_{20}u_1u_2+b_{11}(u_1v_2+u_2v_1)+\frac{1}{2}b_{21}u_1^2v_1+\frac{1}{6}b_{30}u_1^3\\ 0\end{pmatrix}.$$

Next, we separate the time scale for system (16):

$$T_1=\varepsilon t,\ \ T_2=\varepsilon^2 t,\ \ T_3=\varepsilon^3 t,$$

then

$$\frac{\partial}{\partial t}=\varepsilon\frac{\partial}{\partial T_1}+\varepsilon^2\frac{\partial}{\partial T_2}+\varepsilon^3\frac{\partial}{\partial T_3}+o(4). \tag{21}$$

We substitute Eqs. (17)–(21) into Eq. (16), and the following equations can be obtained:
The order of ε:

$$\boldsymbol{L}_{\rm c}\begin{pmatrix}u_1\\ v_1\end{pmatrix}=\boldsymbol{0}. \tag{22}$$

The order of ε^2:

$$\boldsymbol{L}_{\rm c}\begin{pmatrix}u_2\\ v_2\end{pmatrix}=\frac{\partial}{\partial T_1}\begin{pmatrix}u_1\\ v_1\end{pmatrix}-d_1\boldsymbol{M}\begin{pmatrix}u_1\\ v_1\end{pmatrix}-\boldsymbol{h}_2. \tag{23}$$

The order of ε^3:

$$\begin{aligned}\boldsymbol{L}_{\rm c}\begin{pmatrix}u_3\\ v_3\end{pmatrix}=&\frac{\partial}{\partial T_1}\begin{pmatrix}u_2\\ v_2\end{pmatrix}+\frac{\partial}{\partial T_2}\begin{pmatrix}u_1\\ v_1\end{pmatrix}-d_1\boldsymbol{M}\begin{pmatrix}u_2\\ v_2\end{pmatrix}\\ &-d_2\boldsymbol{M}\begin{pmatrix}u_1\\ v_1\end{pmatrix}-\boldsymbol{h}_3.\end{aligned} \tag{24}$$

We can see that $\boldsymbol{L}_{\rm c}$ is the linear operator close to the onset $d=d_{\rm c}$ for the order of ε as in Eq. (22). The form of the solution is as follows:

$$\begin{pmatrix}u_1\\ v_1\end{pmatrix}=\begin{pmatrix}\varphi\\ 1\end{pmatrix}\left(W_1\,{\rm e}^{{\rm i}\boldsymbol{k}_1\cdot\boldsymbol{r}}+W_2\,{\rm e}^{{\rm i}\boldsymbol{k}_2\cdot\boldsymbol{r}}+W_3\,{\rm e}^{{\rm i}\boldsymbol{k}_3\cdot\boldsymbol{r}}\right)+{\rm c.c.}, \tag{25}$$

where $\varphi=-\frac{a_{12}}{a_{11}-D_1\hat{k}_{\rm c}^2}$, $\left|\boldsymbol{k}_j\right|^2=\hat{k}_{\rm c}^2$, c.c. represents the conjugate of the right term, W_j is the amplitude of the mode ${\rm e}^{{\rm i}\boldsymbol{k}_j\cdot\boldsymbol{r}}$ $(j=1,2,3)$ of the system under the first-order perturbation. For the order of ε^2

$$\boldsymbol{L}_{\rm c}\begin{pmatrix}u_2\\ v_2\end{pmatrix}=\frac{\partial}{\partial T_1}\begin{pmatrix}u_1\\ v_1\end{pmatrix}-d_1\begin{pmatrix}0\\ \nabla^2u_1\end{pmatrix}$$

$$-\begin{pmatrix}\frac{1}{2}b_{20}u_1^2+b_{11}u_1v_1\\ 0\end{pmatrix}\triangleq\begin{pmatrix}F_u\\ F_v\end{pmatrix}. \tag{26}$$

The zero eigenvector of $\boldsymbol{L}_{\rm c}^*$ is

$$\begin{pmatrix}1\\ \psi\end{pmatrix}{\rm e}^{-{\rm i}\boldsymbol{k}_j\cdot\boldsymbol{r}}+{\rm c.c.},\ \ j=1,2,3, \tag{27}$$

where $\psi=-\frac{a_{11}-\hat{k}_{\rm c}^2D_1}{a_{21}-d_{\rm c}\hat{k}_{\rm c}^2}$, $\boldsymbol{L}_{\rm c}^*$ is the adjoint operator of $\boldsymbol{L}_{\rm c}$. According to the Fredholm solvability conditions, the vector function of the right term of Eq. (26) must be orthogonal to the zero eigenvectors of $\boldsymbol{L}_{\rm c}^*$, so this equation has the following nontrivial solution:

$$\begin{pmatrix}1 & \psi\end{pmatrix}\begin{pmatrix}F_u^j\\ F_v^j\end{pmatrix}=0,\ \ j=1,2,3, \tag{28}$$

where F_u^j and F_v^j are from F_u and F_v of the coefficient corresponding to ${\rm e}^{{\rm i}\boldsymbol{k}_j\cdot\boldsymbol{r}}$, respectively. We obtain

$$\begin{cases}(\varphi+\psi)\dfrac{\partial W_1}{\partial T_1}=-d_1\varphi\psi\hat{k}_{\rm c}^2W_1+(\varphi^2b_{20}+2\varphi b_{11})\overline{W}_2\overline{W}_3,\\ (\varphi+\psi)\dfrac{\partial W_2}{\partial T_1}=-d_1\varphi\psi\hat{k}_{\rm c}^2W_2+(\varphi^2b_{20}+2\varphi b_{11})\overline{W}_1\overline{W}_3,\\ (\varphi+\psi)\dfrac{\partial W_3}{\partial T_1}=-d_1\varphi\psi\hat{k}_{\rm c}^2W_3+(\varphi^2b_{20}+2\varphi b_{11})\overline{W}_1\overline{W}_2.\end{cases} \tag{29}$$

Substituting Eq. (25) into Eq. (26), we get

$$\begin{aligned}\begin{pmatrix}u_2\\ v_2\end{pmatrix}=&\begin{pmatrix}U_0\\ V_0\end{pmatrix}+\sum_{j=1}^{3}\begin{pmatrix}U_j\\ V_j\end{pmatrix}{\rm e}^{{\rm i}\boldsymbol{k}_j\cdot\boldsymbol{r}}+\sum_{j=1}^{3}\begin{pmatrix}U_{jj}\\ V_{jj}\end{pmatrix}{\rm e}^{{\rm i}2\boldsymbol{k}_j\cdot\boldsymbol{r}}\\ &+\begin{pmatrix}U_{12}\\ V_{12}\end{pmatrix}{\rm e}^{{\rm i}(\boldsymbol{k}_1-\boldsymbol{k}_2)\cdot\boldsymbol{r}}+\begin{pmatrix}U_{23}\\ V_{23}\end{pmatrix}{\rm e}^{{\rm i}(\boldsymbol{k}_2-\boldsymbol{k}_3)\cdot\boldsymbol{r}}\\ &+\begin{pmatrix}U_{31}\\ V_{31}\end{pmatrix}{\rm e}^{{\rm i}(\boldsymbol{k}_3-\boldsymbol{k}_1)\cdot\boldsymbol{r}}+{\rm c.c.}\end{aligned} \tag{30}$$

From Eq. (26), we have $\boldsymbol{L}_{\rm c}\begin{pmatrix}u_2\\ v_2\end{pmatrix}=\begin{pmatrix}F_u\\ F_v\end{pmatrix}$, then we compare the coefficients of terms such as 0, ${\rm e}^{{\rm i}\boldsymbol{k}_j\cdot\boldsymbol{r}}$, ${\rm e}^{{\rm i}2\boldsymbol{k}_j\cdot\boldsymbol{r}}$ and ${\rm e}^{{\rm i}(\boldsymbol{k}_j-\boldsymbol{k}_l)\cdot\boldsymbol{r}}$ in Eq. (26) and obtain

$$\begin{cases}U_0=u_{000}(|W_1|^2+|W_2|^2+|W_3|^2),\\ V_0=v_{000}(|W_1|^2+|W_2|^2+|W_3|^2),\end{cases}\quad U_j=\varphi V_j,$$

$$\begin{cases}U_{jj}=u_{11}W_j^2,\\ V_{jj}=v_{11}W_j^2,\end{cases}\quad\begin{cases}U_{jl}=\widetilde{u}W_j\overline{W}_l,\\ V_{jl}=\widetilde{v}W_j\overline{W}_l,\end{cases}$$

where

$$\begin{cases}u_{000}=\dfrac{a_{22}(b_{20}\varphi^2+2b_{11}\varphi)}{a_{12}a_{21}-a_{11}a_{22}},\\ v_{000}=\dfrac{a_{21}(b_{20}\varphi^2+2b_{11}\varphi)}{a_{11}a_{22}-a_{12}a_{21}},\end{cases}$$

$$\begin{cases}u_{11}=\dfrac{(a_{22}-4\hat{k}_{\rm c}^2D_2)(\frac{1}{2}b_{20}\varphi^2+b_{11}\varphi)}{a_{12}(a_{21}-4d_{\rm c}\hat{k}_{\rm c}^2)-(a_{11}-4\hat{k}_{\rm c}^2D_1)(a_{22}-4\hat{k}_{\rm c}^2D_2)},\\ v_{11}=\dfrac{(a_{21}-4d_{\rm c}\hat{k}_{\rm c}^2)(\frac{1}{2}b_{20}\varphi^2+b_{11}\varphi)}{(a_{11}-4\hat{k}_{\rm c}^2D_1)(a_{22}-4\hat{k}_{\rm c}^2D_2)-a_{12}(a_{21}-4d_{\rm c}\hat{k}_{\rm c}^2)},\end{cases}$$

$$\begin{cases}\widetilde{u}=\dfrac{(a_{22}-3\hat{k}_c^2D_2)(b_{20}\varphi^2+2b_{11}\varphi)}{a_{12}(a_{21}-3d_c\hat{k}_c^2)-(a_{11}-3\hat{k}_c^2D_1)(a_{22}-3\hat{k}_c^2D_2)},\\ \widetilde{v}=\dfrac{(a_{21}-3d_c\hat{k}_c^2)(b_{20}\varphi^2+2b_{11}\varphi)}{(a_{11}-3\hat{k}_c^2D_1)(a_{22}-3\hat{k}_c^2D_2)-a_{12}(a_{21}-3d_c\hat{k}_c^2)}.\end{cases}$$

For the order of ε^3:

$$\begin{aligned}&\boldsymbol{L}_c\begin{pmatrix}u_3\\v_3\end{pmatrix}\\ &=\frac{\partial}{\partial T_1}\begin{pmatrix}u_2\\v_2\end{pmatrix}+\frac{\partial}{\partial T_2}\begin{pmatrix}u_1\\v_1\end{pmatrix}-d_1\begin{pmatrix}0\\\nabla^2u_2\end{pmatrix}-d_2\begin{pmatrix}0\\\nabla^2u_1\end{pmatrix}\\ &\quad-\begin{pmatrix}b_{20}u_1u_2+b_{11}(u_1v_2+u_2v_1)+\dfrac{1}{2}b_{21}u_1^2v_1+\dfrac{1}{6}b_{30}u_1^3\\0\end{pmatrix}\\ &\triangleq\begin{pmatrix}G_u\\G_v\end{pmatrix}.\end{aligned}\tag{31}$$

The coefficient of the term $e^{i\boldsymbol{k}_1\cdot\boldsymbol{r}}$ in Eq. (31) is $(G_u^1,G_v^1)^{\mathrm{T}}$:

$$\begin{aligned}G_u^1&=\varphi\frac{\partial V_1}{\partial T_1}+\varphi\frac{\partial W_1}{\partial T_2}-\Big[(b_{20}\varphi+b_{11})\big(u_{000}(|W_1|^2+|W_2|^2+|W_3|^2)W_1+\varphi\overline{W}_2\overline{V}_3+\varphi\overline{V}_2\overline{W}_3\\&\quad+u_{11}W_1^2\overline{W}_1+\widetilde{u}W_1\overline{W}_2W_2+\widetilde{u}W_1\overline{W}_3W_3\big)+b_{11}\varphi\big(v_{000}(|W_1|^2+|W_2|^2+|W_3|^2)W_1\\&\quad+\overline{W}_2\overline{V}_3+\overline{V}_2\overline{W}_3+v_{11}|W_1|^2\overline{W}_1+\widetilde{v}W_1\overline{W}_2W_2+\widetilde{v}W_1\overline{W}_3W_3\big)+(\frac{1}{2}b_{21}\varphi^2v_1^3+\frac{1}{6}b_{30}\varphi^3)(3|W_1|^2+6|W_2|^2+6|W_3|^2)W_1\Big]\\&=\varphi\frac{\partial V_1}{\partial T_1}+\varphi\frac{\partial W_1}{\partial T_2}+(I_1|W_1|^2+I_2(|W_2|^2+|W_3|^2))W_1-(b_{20}\varphi^2+2b_{11}\varphi)(\overline{W}_2\overline{V}_3+\overline{V}_2\overline{W}_3),\\G_v^1&=\frac{\partial V_1}{\partial T_1}+\frac{\partial W_1}{\partial T_2}+d_1\hat{k}_c^2\varphi V_1+d_2\hat{k}_c^2\varphi W_1,\end{aligned}$$

where

$$\begin{aligned}I_1&=-(b_{20}\varphi+b_{11})(u_{000}+u_{11})-b_{11}\varphi(v_{000}+v_{11})\\&\quad-\frac{3}{2}b_{21}\varphi^2-\frac{1}{2}b_{30}\varphi^3,\\I_2&=-(b_{20}\varphi+b_{11})(u_{000}+\widetilde{u})-b_{11}\varphi(v_{000}+\widetilde{v})\\&\quad-3b_{21}\varphi^2-b_{30}\varphi^3.\end{aligned}$$

G_u^2, G_v^2, G_u^3 and G_v^3 can be obtained by changing the subscripts of W and V. Then we continue to use the Fredholm solvability conditions

$$\begin{pmatrix}1&\psi\end{pmatrix}\begin{pmatrix}G_u^j\\G_v^j\end{pmatrix}=0,\quad j=1,2,3.$$

We can write one of the equations as follows, then it is easy to get the other equations by transforming the subscripts:

$$\begin{cases}(\varphi+\psi)(\dfrac{\partial V_1}{\partial T_1}+\dfrac{\partial W_1}{\partial T_2})=-\varphi\psi\hat{k}_c^2(d_1V_1+d_2W_1)+(\varphi^2b_{20}+2\varphi b_{11})(\overline{W}_2\overline{V}_3+\overline{V}_2\overline{W}_3)-(I_1|W_1|^2+I_2(|W_2|^2+|W_3|^2))W_1,\\(\varphi+\psi)(\dfrac{\partial V_2}{\partial T_1}+\dfrac{\partial W_2}{\partial T_2})=-\varphi\psi\hat{k}_c^2(d_1V_2+d_2W_2)+(\varphi^2b_{20}+2\varphi b_{11})(\overline{W}_3\overline{V}_1+\overline{V}_3\overline{W}_1)-(I_1|W_2|^2+I_2(|W_1|^2+|W_3|^2))W_2,\\(\varphi+\psi)(\dfrac{\partial V_3}{\partial T_1}+\dfrac{\partial W_3}{\partial T_2})=-\varphi\psi\hat{k}_c^2(d_1V_3+d_2W_3)+(\varphi^2b_{20}+2\varphi b_{11})(\overline{W}_1\overline{V}_2+\overline{V}_1\overline{W}_2)-(I_1|W_3|^2+I_2(|W_1|^2+|W_2|^2))W_3.\end{cases}\tag{32}$$

Step 3 Supposing

$$A_j=\varepsilon W_j+\varepsilon^2V_j+o(3),$$

according to Eq. (21) we have the amplitude equation of A_j:

$$\frac{\partial A_j}{\partial t}=\varepsilon\frac{\partial A_j}{\partial T_1}+\varepsilon^2\frac{\partial A_j}{\partial T_2}+o(3).\tag{33}$$

From the above conclusions, we get the amplitude equations as follows:

$$\begin{cases}s_0\dfrac{\partial A_1}{\partial t}=\mu A_1+h\overline{A}_2\overline{A}_3-(g_1|A_1|^2+g_2(|A_2|^2+|A_3|^2))A_1,\\s_0\dfrac{\partial A_2}{\partial t}=\mu A_2+h\overline{A}_1\overline{A}_3-(g_1|A_2|^2+g_2(|A_1|^2+|A_3|^2))A_2,\\s_0\dfrac{\partial A_3}{\partial t}=\mu A_3+h\overline{A}_1\overline{A}_2-(g_1|A_3|^2+g_2(|A_1|^2+|A_2|^2))A_3,\end{cases}\tag{34}$$

where

$$s_0=\frac{\varphi+\psi}{\varphi\psi\hat{k}_c^2d_c},\quad\mu=\frac{d-d_c}{d_c},\quad h=-\frac{\varphi^2b_{20}+2\varphi b_{11}}{\varphi\psi\hat{k}_c^2d_c},$$
$$g_1=-\frac{I_1}{\varphi\psi\hat{k}_c^2d_c},\quad g_2=-\frac{I_2}{\varphi\psi\hat{k}_c^2d_c}.$$

Next, we analyze the stability of the amplitude Eq. (34). Each amplitude in the above equations can be expressed as follows:

$$A_j=\rho_je^{i\theta_j},\quad j=1,2,3,\tag{35}$$

where $\rho_j=|A_j|$ represents mode and θ_j represents the corresponding phase angle. Substituting Eq. (35) into Eq. (34) and separating the real and imaginary parts for comparison, one

can obtain

$$\begin{cases} s_0\dfrac{\partial\theta}{\partial t} = -h\dfrac{\rho_2^2\rho_3^2+\rho_1^2\rho_3^2+\rho_1^2\rho_2^2}{\rho_1\rho_2\rho_3}\sin\theta, \\ s_0\dfrac{\partial\rho_1}{\partial t} = \mu\rho_1 + h\rho_2\rho_3\cos\theta - g_1\rho_1^3 - g_2(\rho_2^2+\rho_3^2))\rho_1, \\ s_0\dfrac{\partial\rho_2}{\partial t} = \mu\rho_2 + h\rho_1\rho_3\cos\theta - g_1\rho_2^3 - g_2(\rho_1^2+\rho_3^2))\rho_2, \\ s_0\dfrac{\partial\rho_3}{\partial t} = \mu\rho_3 + h\rho_1\rho_2\cos\theta - g_1\rho_3^3 - g_2(\rho_1^2+\rho_2^2))\rho_3, \end{cases} \tag{36}$$

where $\theta=\theta_1+\theta_2+\theta_3$; clearly $\mu>0$. To guarantee the existence of the steady-state solution of Eq. (36), the coefficients of g_1 and g_2 must be positive. Moreover, $g_2>g_1>0$.

Theorem 4

(1) The homogeneous steady state:

$$\rho_1=\rho_2=\rho_3=0,$$

which is stable when $\mu<0$ and unstable when $\mu>0$.

(2) Stripe pattern S:

$$\rho_1=\sqrt{\frac{\mu}{g_1}},\quad \rho_2=\rho_3=0,$$

which is stable when $\mu>\mu_2=\frac{h^2g_1}{(g_2-g_1)^2}$ and unstable when $\mu<\mu_2$.

(3) Hexagonal pattern H_0 or H_π with $\theta=0$ or $\theta=\pi$:

$$\rho_1=\rho_2=\rho_3=\frac{|h|\pm\sqrt{h^2+4(g_1+2g_2)\mu}}{2(g_1+2g_2)},$$

(this exists only if $\mu>\mu_1=\frac{-h^2}{4(g_1+2g_2)}$).

For the steady-state solution $\rho^-=\frac{|h|-\sqrt{h^2+4(g_1+2g_2)\mu}}{2(g_1+2g_2)}$ the corresponding pattern is always unstable.

For the steady-state solution $\rho^+=\frac{|h|+\sqrt{h^2+4(g_1+2g_2)\mu}}{2(g_1+2g_2)}$ the corresponding pattern is stable when $\mu<\mu_3=\frac{h^2(2g_1+g_2)}{(g_2-g_1)^2}$.

(4) The mixed state:

$$\rho_1=\frac{|h|}{g_2-g_1},\quad \rho_2=\rho_3=\sqrt{\frac{\mu-g_1\rho_1^2}{g_1+g_2}},$$

is always unstable when $g_2>g_1$ and $\mu>\mu_2$.

To sum up, when we change the value of the cross-diffusion coefficient d and fix the other parameters in the system (3), we can calculate the value of h, μ, μ_1, μ_2 and μ_3, and we have $\mu_1<0<\mu_2<\mu_3$.

Theorem 5

(1) If $h>0$, then the hexagonal pattern is shown as $H_0(\theta=0)$, while H_π is always unstable; if $h<0$, then the hexagonal pattern is shown as $H_\pi(\theta=\pi)$, while H_0 is always unstable.

(2) When $\mu\in(\mu_1,0)$, the homogeneous steady state and the hexagonal pattern are stable; when $\mu\in(0,\mu_2)$, the hexagonal pattern is stable, but the homogeneous steady state and the stripe pattern are unstable; when $\mu\in(\mu_2,\mu_3)$, the stripe pattern and the hexagonal pattern are stable, but the homogeneous steady state is unstable; when $\mu\in(\mu_3,\infty)$, the stripe pattern is stable, but the homogeneous steady state and the hexagonal pattern are unstable.

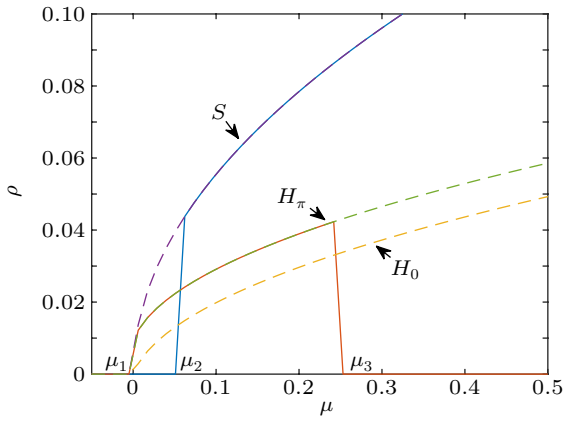


Fig. 2. The bifurcation diagram of the amplitude Eq. (34). Here S represents the stripe pattern; H_0 represents the hexagonal pattern with $\theta=0$; H_π represents the hexagonal pattern with $\theta=\pi$. The solid line is the stable state; the dotted line is the unstable state.

4. Numerical simulation

In this section, we use MATLAB to simulate system (3) in two dimensions. To analyze the dynamic behavior of the system, we study it on discrete grids of 100×100 with Neumann boundary conditions, and take the space step as 1 and the time step as 0.01. As is well known, the system dynamics are determined by the initial conditions. The species distribution will always be uniform if the initial spatial distribution of plant and wrack is uniform; however, we are interested in random perturbations of the initial conditions around a uniform distribution of the unique positive equilibrium $E_*=(u_*,u_*)$. In the numerical simulation, we observe different types of patterns, and the distributions of plant and wrack are always the same types of patterns. Therefore, we only show the pattern formation for plant biomass $u(t,x,y)$ in our numerical simulations.

In the following, we show the different types of patterns due to the variation of the cross-diffusion coefficient d. Among the parameter values of system (3), we selected the three sets of parameter values shown in Table 1. Then we obtained the unique positive equilibrium $E_*=(1.8642,1.8642)$ of system (3) and the critical value of the Turing bifurcation as $d_c=2.26427$. We get $h=-1.6092$, $g_1=32.4881$, $g_2=70.3498$, $\mu_1=-0.0037$, $\mu_2=0.0587$ and $\mu_3=0.2445$. From the previous analysis, we know that the values in Table 1 satisfy condition (2) of Theorem 3, namely, the only positive equilibrium E_* is unstable and Turing instability occurs at $d>d_c$.

First, we take $d=2.3238$, satisfying this parameter condition. Condition (2) of Theorem 3 holds and Turing instability

occurs. Further, we can calculate that at this point $\mu = 0.0263$ belongs to $(0, \mu_2)$, and according to the conclusion of Theorem 5, system (3) will form a hexagonal pattern and be stable. From the simulations, we can see that a hexagonal pattern gradually forms as time t increases (see Fig. 3).

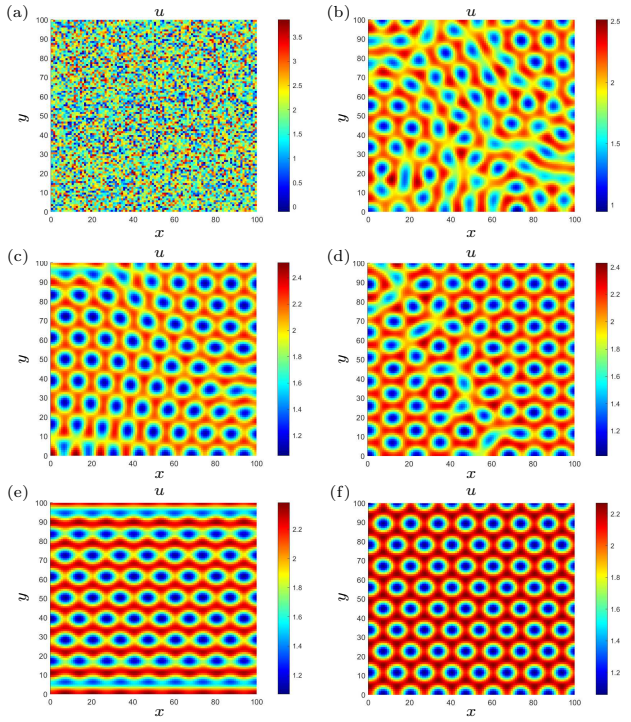


Fig. 3. (a) $t = 0$, (b) $t = 1000$, (c) $t = 4000$, (d) $t = 6000$, (e) $t = 9000$, (f) $t = 12000$. The system parameters are listed in Table 1.

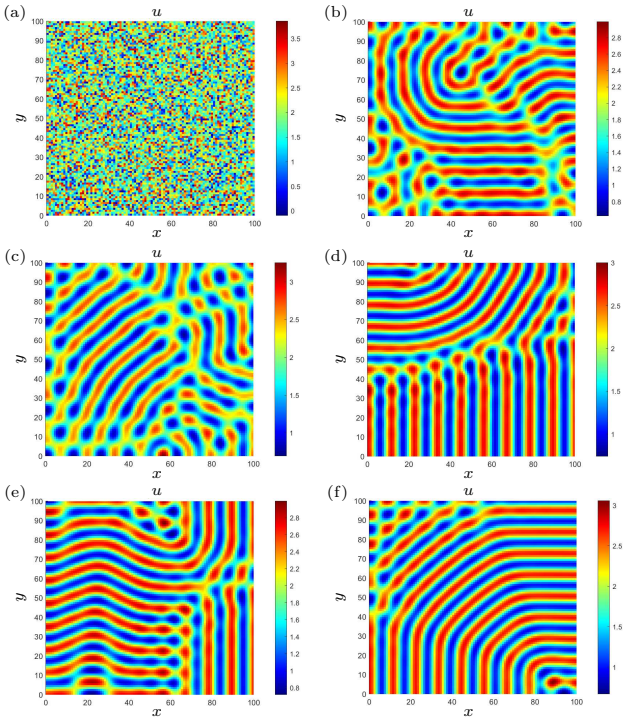


Fig. 4. (a) $t = 0$, (b) $t = 500$, (c) $t = 1000$, (d) $t = 3000$, (e) $t = 8000$, (f) $t = 10000$. The system parameters are listed in Table 1.

Next, we take $d = 2.4728$, which satisfies condition (2) of Theorem 3, at which point Turing instability occurs. It is calculated that $\mu = 0.0921$ belongs to (μ_2, μ_3), and according to the conclusion of Theorem 5, the hexagonal pattern and stripe pattern are stable. In the numerical simulations, as time t grows, We can observe a mixture state of hexagonal and stripe patterns, as shown in Fig. 4.

Finally, we take $d = 2.8503$, and satisfying this parameter condition, condition (2) of Theorem 3 holds, which tells us that Turing instability will occur and $\mu = 0.2588$ belongs to (μ_3, ∞). We get a stable stripe pattern according to the conclusion of Theorem 5. By numerical simulation, we find that the stripe pattern gradually forms as time t increases (see Fig. 5).

In summary, the numerical simulation verifies our theoretical results.

Table 1. Parameter values in Figs. 3–5.

	k_3	A	K	D_1	D_2	d
Fig. 3	1.5	0.8	10	1	6	2.3238
Fig. 4	1.5	0.8	10	1	6	2.4728
Fig. 5	1.5	0.8	10	1	6	2.8503

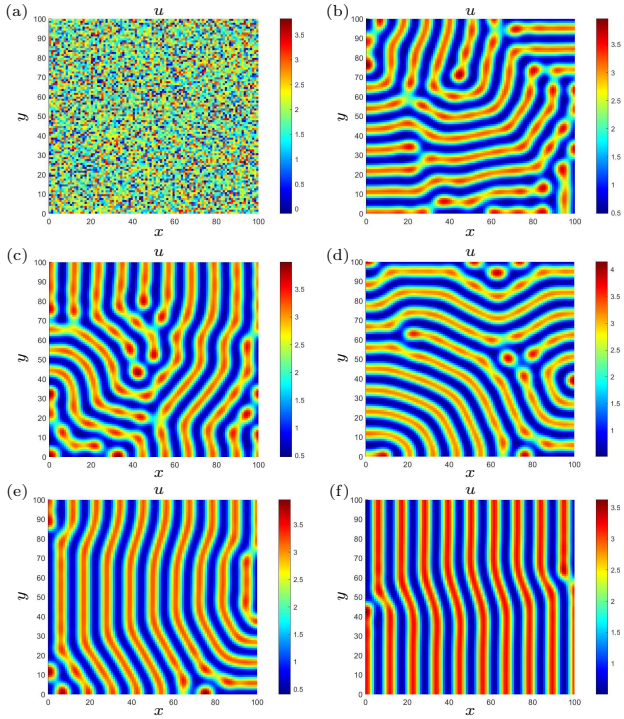


Fig. 5. (a) $t = 0$, (b) $t = 500$, (c) $t = 1000$, (d) $t = 3000$, (e) $t = 8000$, (f) $t = 12000$. The system parameters are listed in Table 1.

5. Conclusion

In this paper we study the Turing instability and pattern formation mechanism of a plant–wrack model with both self-diffusion and cross-diffusion terms, and conduct theoretical analysis and numerical simulation of this model. It is found that the formation of spatial patterns induced by cross-diffusion has an important influence on pattern selection. The theoretical and numerical simulation results show that the plant–wrack system (3) with cross-diffusion exhibits

a very rich dynamic behavior. As the cross-diffusion coefficient d changes, the system will have different types of pattern structure: when the cross-diffusion coefficient d belongs to $(d_c, d_c + d_c\mu_2)$, the distribution of plant presents hexagonal patterns (see Fig. 3). When d belongs to $(d_c + d_c\mu_2, d_c + d_c\mu_3)$, mixtures of hexagonal and stripe patterns appear (see Fig. 4). When the cross-diffusion coefficient d belongs to $(d_c + d_c\mu_3, \infty)$, we obtain stripe patterns (see Fig. 5).

Acknowledgments

Project supported by the National Natural Science Foundation of China (Grant Nos. 10971009, 11771033, and 12201046), Fundamental Research Funds for the Central Universities (Grant No. BLX201925), and China Postdoctoral Science Foundation (Grant No. 2020M670175).

References

[1] Wang D 1990 *Advances in Math* **19** 38
[2] Zhang C X and Ouyang Q 2002 *Science (Shanghai)* **75** 17
[3] Turing A M 1952 *Bulletin of Mathematical Biology* **641** 37
[4] Marsden J E and McCracken M 1978 *Springer-Verlag, New York* **20** 410
[5] Wiggins 1991 *New York: Springer-Verlag* **31** 1
[6] Murray J D 2002 *Springer-Verlag, New York* **17** 187
[7] Zheng L X, Guo B Z and Yan L 2019 *Acta Phys. Sin.* **68** 068201 (in Chinese)
[8] Qi Q, Zhang D J, Zhang M Y, Tong S Z and Zhu G L 2021 *STE* **780** 146630
[9] Koppel J V D and Crain C M 2006 *The American Naturalist* **168** 136
[10] Yu B G 2010 *Commun Nonlinear Sci Numer Simulat* **15** 2201
[11] Liu Z H, Wang A L, Wang B and Liu Y J 2010 *AMC* **216** 983
[12] Wang J L, Li Y and Hou X J 2019 *Mathematical Analysis* **26** 231
[13] Hou X J, Wang J L and Li Y 2019 *Applicable Analysis* **101** 2022
[14] Li Y, Cao J, Sun Y, Song D and Wu X 2021 *ADE* **539** 399
[15] Zhou J 2016 *Mathematical Biosciences and Engineering* **13** 857
[16] Kerner E H 1957 *Bull. Math. Biol.* **19** 121
[17] Holmes E E, Lewis M A, Banks J E and Veit R R 1994 *Ecol.* **75** 17
[18] Chattopadhyay J and Tapaswi P K 1997 *Acta Appl. Math.* **48** 112
[19] Okubo A and Levin S 2001 *Springer, Berlin* **14** 591
[20] Xie Z 2012 *J. Math. Anal. Appl.* **388** 539
[21] Guin L N, Haque M and Mandal P K 2012 *Appl. Math. Model.* **36** 1825
[22] Guin L N 2014 *Appl. Math. Comput.* **226** 320
[23] Haile D and Xie Z 2015 *Math. Biosci.* **267** 134
[24] Fang L and Wang J 2016 *Appl. Math. Lett.* **58** 49
[25] Ghorai S and Poria S 2016 *Chaos Solit. Fract.* **91** 421
[26] Wen Z and Fu S M 2016 *Chaos Solit. Fract.* **91** 379
[27] Iida M, Mimura M and Ninomiya H 2006 *JMB* **53** 617
[28] Banerjee M, Ghorai S, Mukherjee and Nayana 2018 *AMM* **55** 383
[29] Li L, Jin Z and Sun G Q 2008 *Chin. Phys. Lett.* **25** 3500
[30] Wang W M, Wang W J, Lin Y Z and Tan Y J 2011 *Chin. Phys. B* **20** 034702
[31] Banerjee M and Abbas S 2015 *Ecological Complexity* **21** 199
[32] Han R J and Dai B X 2017 *IJBC* **27** 1750088
[33] Sun G Q, Wang C H and Wu Z Y 2017 *Nonlinear Dyn* **88** 1385
[34] Zheng Q Q, Wang Z J and Shen J W 2017 *Chin. Phys. B* **26** 020501
[35] Zheng Q Q and Shen J W 2020 *Applied Mathematics and Computation* **381** 125304
[36] Batabyal S, Jana D and Upadhyay R 2021 *CSF* **147** 110929
[37] Arnab M, Ranjit K, Argha M and Sanjeev K 2022 *AMC* **423** 127010